Toward Robotic Pseudodynamic Testing for Hybrid Simulations of Air-to-Air Refueling

Mario Bolien, Pejman Iravani, and Jonathan Luke du Bois

***Abstract*—Hybrid simulation couples experimental tests of novel components to validated numerical models of the remainder of a system and provides high-confidence predictions of their coupled dynamic behavior. Air-to-air refueling (AAR) is an example of the type of system that can benefit from this development approach. The work in this paper concerns the on-ground validation and preflight verification of probe–drogue contact–impact scenarios in AAR maneuvers using off-the-shelf multiaxis industrial robots as part of a hybrid test to interface the refueling hardware with numerical models of the flight environment. While industrial manipulators present a cost-effective solution, bandwidth and power limitations inevitably cause practical problems for real-time hybrid testing. These deficiencies typically manifest themselves as significant tracking inaccuracies or instabilities when sharp nonlinearities or discontinuities are encountered as part of a contact phase. Here, the novel robotic pseudodynamic testing (RPsDT) method is employed to circumvent the contact-response speed limitations of industrial robots. This paper presents and discusses the application of RPsDT to contact–impact problems, outlines the challenges and limitations of the technique in an easily reproducible validation experiment, and details the first RPsDT hybrid simulation of an AAR maneuver using scaled refueling hardware. It is concluded that RPsDT provides a useful tool for the investigation of a particular subclass of multibody contact–impact problems including AAR, where the response of the contacting structures does not possess significant rate-of-loading effects. Future work will comprise tests with full-scale AAR hardware.**

***Index Terms*—Air-to-air refueling, contact dynamics, hybrid testing, robotic pseudodynamic testing (RPsDT).**

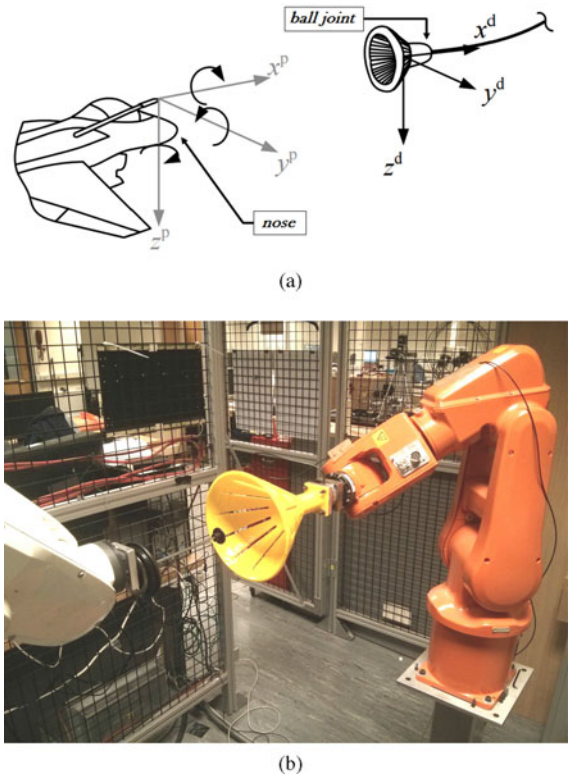

Fig. 1. (a) Schematic of a probe–drogue AAR system including frame assignment for receiver and drogue. Tanker and tow-point frame (not shown) comply with steady-state orientation of the drogue frame. (b) Setup for reduced-scale testing of probe–drogue contact–impact scenarios in AAR.

I. Introduction

AIR-TO-AIR refueling (AAR) provides a means for extending the range, payload, and endurance of aircraft and increases efficiency through the elimination of the large fuel consumption in repeated takeoff and landing operations [1]. The work documented here is concerned with probe and drogue refueling, where the tanker trails a flexible hose equipped with a coupling and drogue assembly [see Fig. 1(a)]. The receiver aircraft is equipped with a probe, rigidly mounted to the aircraft, which is maneuvered by the pilot to engage the drogue.

The emergence of unmanned aerial vehicles brings the prospect of aircraft staying airborne indefinitely, supported by autonomous AAR so that landing becomes necessary for maintenance only. Consequently, reliable tools for the on-ground validation and preflight verification of docking maneuvers are widely regarded as an important enabling technology. The complexity of an AAR environment demands the development of special techniques to satisfy this need, and hybrid testing is one such tool.

Hybrid testing allows for representative conditions in a repeatable laboratory-based setup and provides a valuable intermediate derisking step between component testing and full system

Manuscript received July 25, 2016; revised October 25, 2016; accepted November 30, 2016. Date of publication January 23, 2017; date of current version April 14, 2017. Recommended by Technical Editor Z. Xiong. This work was supported by Cobham Mission Systems, and by the U.K. Engineering and Physical Sciences Research Council under Grant EP/L504890/1.

The authors are with the Department of Mechanical Engineering, University of Bath, Bath BA2 7AY, U.K. (e-mail: M.Bolien@bath.ac.uk; P.Iravani@bath.ac.uk; J.L.du.Bois@bath.ac.uk).

Color versions of one or more of the figures in this paper are available online at http://ieeexplore.ieee.org.

Digital Object Identifier 10.1109/TMECH.2016.2644200

flight testing. Hybrid tests are comprised of two domains: 1) the physical domain where real components are evaluated experimentally; and 2) the numerical domain where computer models simulate the response of the remainder of the system. The two domains are coupled together to reproduce the transient and/or nonlinear behavior of the complete emulated system.

The use of industrial robots as a cost-effective means for relative motion reproduction has been a popular choice for hybrid tests of both AAR scenarios [2] and the related application of satellite docking [3].

Actuators for real-time (RT) hybrid testing must be accurate and fast so as to minimize the influence of the actuator transfer dynamics. While contemporary industrial robots satisfy the first criterion, they fall short of the latter, especially for high-velocity impacts and stiff collisions such as those experienced in AAR contact scenarios. The main limitations for satisfactory response speeds and RT performance result from the large link inertias as well as proprietary control architectures that are optimized for precision in repetitive positioning tasks. The latter typically preclude low-level access to the axis controller such that favorable RT control schemes such as impedance control [4], passivity-based control [5], or model inversion schemes [6] cannot be easily realized. High-level proprietary interfaces provide low controller sample rates and considerable dead times in command execution: typically 10–120 ms, and upwards. These dead times have detrimental effects on the fidelity and, critically, the stability of a hybrid test [7]. Typical approaches for mitigation of these effects include forward predictive methods [8], as well as delay and lag compensation [9]. The latter often suffer from demand saturation, and efforts have been made to compensate for this with model-predictive control [10]. All of these approaches work best for a linear plant response and cannot compensate for significant nonlinearities or discontinuous behavior without *a priori* knowledge of the physical system being tested. The existence of reliable models for the physical system would, however, render the hybrid test largely obsolete.

These problems have been approached in a variety of ways. Ma *et al.* [3] realized an admittance control scheme around the proprietary architecture of a KUKA industrial controller for the hardware-in-the-loop (HIL) simulation of satellite docking maneuvers. These maneuvers occur at speeds of the order of centimeters per second so delay and sample rates in the robot control interface did not present a limiting factor. Blomdell *et al.* [11] created an application for motion control of ABB robots, which intercepts and overwrites the messages exchanged between the high-level computer and the low-level axis controller. This grants access to position and velocity reference and feedback signals with low latency and high rates (∼250 Hz), sufficient to perform HIL tests of tracking sensors and control systems for automated AAR procedures [12], [13]. The aircraft, hose/drogue, sensor, and flight controller dynamics are faithfully simulated using this system, but the performance still falls short of that required for the stiff fast contact dynamics as the probe engages the drogue assembly [14].

The work in this paper investigates methods at reduced scale [see Fig. 1(b)] for simulating probe–drogue contact–impact events with hybrid tests. This is done with a view to extending the simulation capabilities of the systems described by du Bois *et al.* [12]. The approach taken is to employ pseudodynamic (PsD) testing in place of RT methods for the duration of the contact event. The PsD method enables dynamic testing on an expanded time scale, thus mitigating instabilities arising through actuator delays. This paper expands upon the robotic pseudodynamic testing (RPsDT) method first outlined in [15] by the present authors and, then, goes on to demonstrate its application in reduced-scale AAR experiments as a precursor to future full-scale tests. This paper provides the first comprehensive work that outlines the motivation, application, and validation of RPsDT, and demonstrates the application of RPsDT to hybrid testing of probe–drogue contact–impact scenarios in an AAR environment. The work seeks to provide valuable contributions to the study of multibody contact–impact problems taking place in complex environmental settings.

This paper is divided into the following parts. Section II describes the RPsDT method including system architecture considerations and implementations from a control perspective. Section III validates RPsDT in an easily reproducible drop-test experiment that was specifically designed to emphasize the remaining challenges and methodical limitations of the technique. This section also builds an argument for the applicability of RPsDT to probe–drogue contact–impact scenarios in AAR, which are then demonstrated and investigated in Section IV. Conclusions are drawn and future work is outlined in Section V.

II. RPsDT of Contact Scenarios

PsD testing was originally developed for the assessment of structural responses to earthquakes in civil engineering [16]. Throughout a PsD test, the specimen is subjected to a displacement history as specified by the simulated environment. In each time step, the displacement is imposed onto the structure in a quasi-static fashion, i.e., non-RT. Physical measurements of the specimen's restoring force are acquired at static equilibrium points and fed back into the simulation. The technique predates current state-of-the-art RT dynamic substructuring methods, but circumvents some of their shortcomings to enable dynamic hybrid testing on an expanded time scale. The actuators require suitable load ratings, but the constraints on bandwidth, response speeds, and power ratings are relaxed [17]. The drawback is the loss of rate-dependent load effects from the physical domain.

PsD testing has been shown to be an effective technique for the investigation of component behavior, for which rate-dependent effects are either easily modeled or negligible compared to dominant elastic/plastic forces [17]. The application of this technique to contact testing circumvents the response time and transfer dynamics issues of industrial robots from the outset at the expense of neglecting time-dependent test characteristics. To the best of the authors' knowledge, neither the application of the PsD test method to contact–impact problems nor the realization of robot-assisted PsD testing has been explored in the academic literature prior to the preliminary results arising from the present work [15].

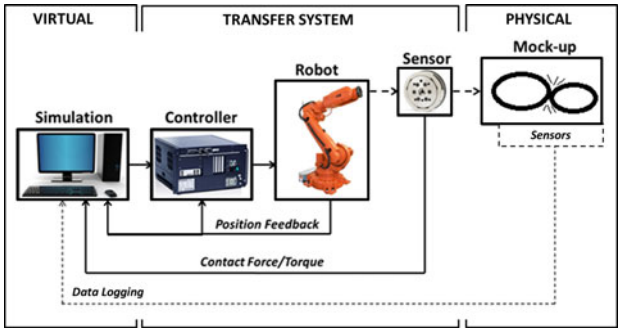

Fig. 2. RPsDT hardware architecture.

A. RPsDT Method

System hybridization for RPsDT is performed according to the same principle as for PsD testing: The system under investigation is broken up into an experimental and a numerically simulated substructure. For RPsDT of contact scenarios, the experimental substructure would typically consist of exactly those components that make physical contact in the real system. The numerical simulation computes the positional response to the combination of measured interface forces and numerically simulated forces. The transfer system consists of an industrial robot equipped with a 6-degree-of-freedom (DOF) force/torque sensor at its end effector. As in standard hybrid tests, additional sensors may be fitted directly to the physical hardware for the purpose of further data acquisition throughout the study. The fundamental RPsDT architecture then complies with the schematic in Fig. 2.

RPsDT of contact scenarios follows the algorithm depicted in Fig. 3. As opposed to standard PsD tests, data from the experimental specimen is not acquired in every time step but only throughout the contact- and near-contact phase, which can be identified based on kinematic constraints in simulation. If in contact, the robot is quasi-statically moved to reproduce the relative position and orientation of the colliding structures. This strains the specimen and allows measurement of the restoring forces and moments, which are then fed back into the simulation. In a noncontact phase, the robot is kept stationary and the simulation can advance immediately without prior contact force acquisition. Upon acquisition of the restoring force, the simulation is treated as an initial value problem: Based on the current states of the contacting structures and physically acquired force measurements from the experimental substructure, the new accelerations are computed and the new system states are obtained with a suitable integration algorithm. The cycle then repeats with the next time step.

B. RPsDT Architecture

The RPsDT method is implemented on a KUKA KR 5 sixx R650 industrial robot controlled via the KUKA robot sensor interface (RSI). Among other control modes, RSI enables the exchange of joint velocity reference commands and joint position feedback between an external PC and the proprietary industrial controller at a sample rate of 12 ms with soft-RT determinism. Our experiments show that the low-level implementation of motor and motion controller execute the reference commands with a considerable delay of 120 ms but achieve accurate demand tracking so long as any form of limit saturation is avoided. This is in agreement with the findings in [18].

The high-level RPsDT architecture is shown in Fig. 4(a). The architecture comprises an offline environment for the numerical simulation and Cartesian-space motion planning as well as an online state -machine-based safety and supervisory logic controller (SSLC) and a joint-space command generator. Both the SSLC and the command generator are embedded in a soft-RT task, and the underlying state machine is directly invokable from the offline simulation environment. To this end, the data exchange between simulation environment and online robot motion controller is kept entirely event based using a fixed transmission control protocol connection that guards the application from unreliability associated with the network protocol. This effectively implements a master–slave hierarchy that completely decouples the simulation from robot motion execution, which has the advantage that robot controller update rates can be met regardless of the computational time required by the simulation, and hence, numerical models can be of almost arbitrarily high fidelity. By contrast, force/torque measurements acquired with the open-source ICub IIT 6DOF FT sensor are fed into the soft-RT task as a continuous stream of datagrams using nonblocking UDP-based interprocess communication so that the SSLC can quickly detect force limit violations and respond with minimal delay. This architecture effectively enslaves the transfer system (robot and controller) and thereby embeds an experimental contact test into the loop of a master simulation. That is, at each simulation time step, the robot can be ordered to pseudodynamically reproduce the relative motion of the contacting structures to acquire and feed back the current contact force such that the following simulation steps become a function of numerically modeled and experimentally measured data.

C. Motion Control

Relative motion reproduction of the physical hardware specimens throughout contact requires manipulation along the shortest path in Cartesian space, i.e., the "tool" must translate along a straight line between demand and target position, while "tool orientation" must simultaneously change from initial to target orientation along the shortest arc (on the surface of a unit sphere). This demand is satisfied by independently planned Cartesian space trajectories for tool translation and orientation. Hence, translation trajectories are specified as cubic polynomials, which accommodate position and zero-velocity boundary conditions for the point-to-point (P2P) motions [see (1)], while intermediate orientations q_{int} follow from the standard textbook definition of spherical linear interpolation (SLERP) [19] between start and target quaternions q_{start} and q_{target}, as per (2). Here, $\Omega = \arccos(q_{\text{start}} \cdot q_{\text{target}})$ describes the angle subtended by the arc of rotation, and the scale factor $s(t)$ is computed as the linear time function $s(t) = \frac{t}{t_{\text{exc}}}$, where t_{exc} represents the total trajectory execution time, as shown in Fig. 5, and t is the time

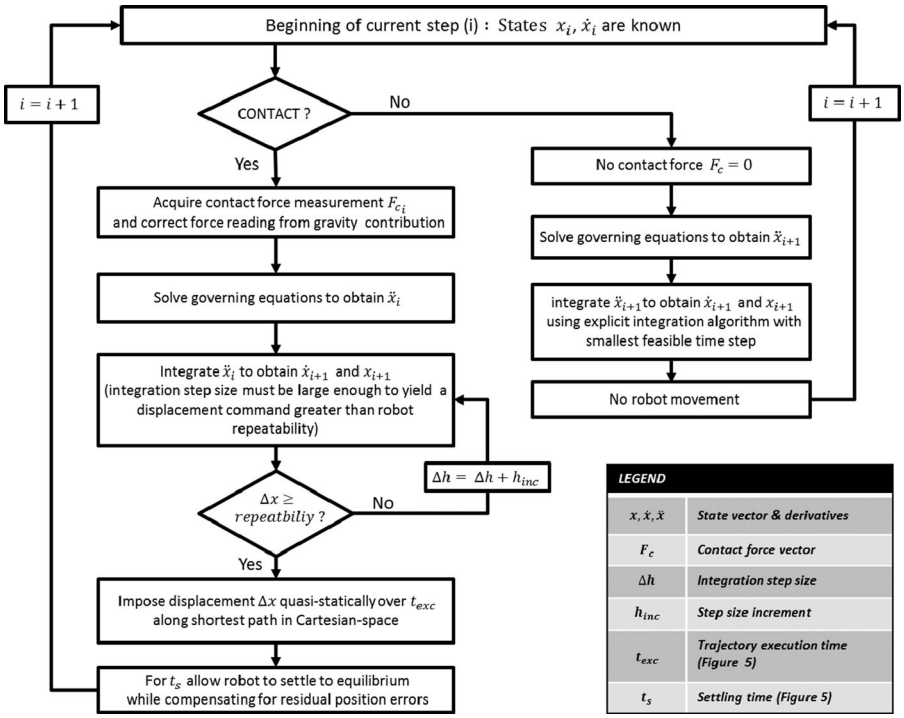

Fig. 3. Algorithmic procedure for RPsDT of contact scenarios.

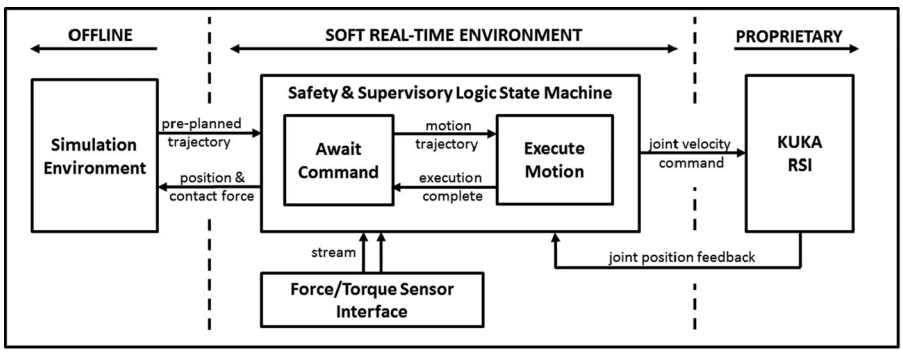

(a)

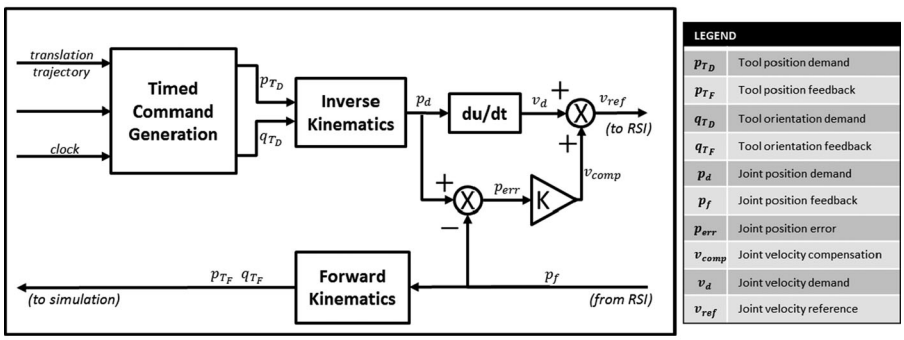

(b)

Fig. 4. (a) High-level RPsDT software architecture. (b) RPsDT motion command generator.

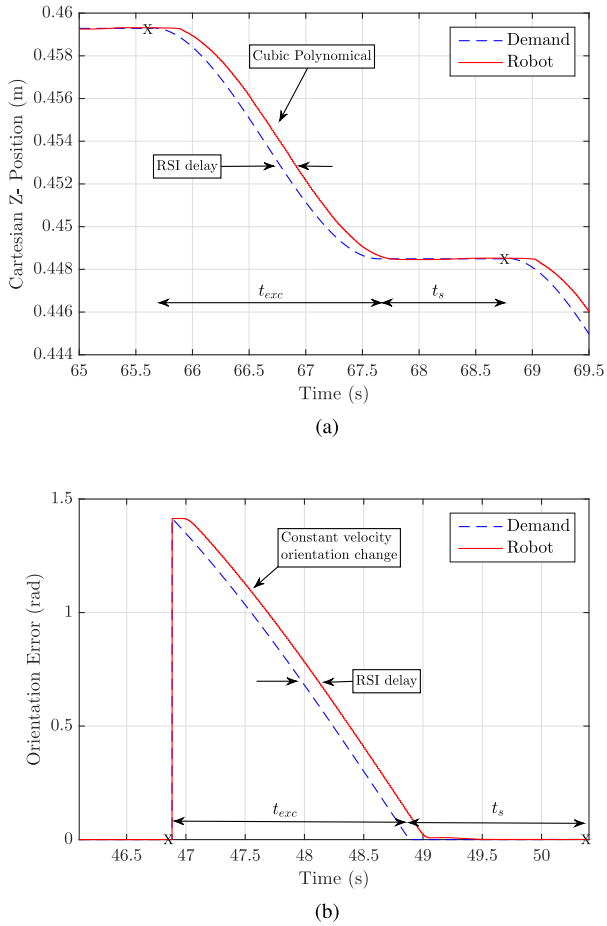

Fig. 5. Examples of quasi-static trajectories showing (a) end effector translation and (b) SLERP-based end effector orientation change. Trajectory execution time, settling time, and points of contact force measurement are identified by "t_{exc}," "t_s," and "*X*," respectively.

from start of the motion

$$\begin{bmatrix} x_{\mathrm{tool}}(t) \\ y_{\mathrm{tool}}(t) \\ z_{\mathrm{tool}}(t) \end{bmatrix} = \begin{bmatrix} a_{x0} \\ a_{y0} \\ a_{z0} \end{bmatrix} + \begin{bmatrix} a_{x1} \\ a_{y1} \\ a_{z1} \end{bmatrix} t + \begin{bmatrix} a_{x2} \\ a_{y2} \\ a_{z2} \end{bmatrix} t^2 + \begin{bmatrix} a_{x3} \\ a_{y3} \\ a_{z3} \end{bmatrix} t^3 \tag{1}$$

$$q_{\mathrm{int}}(t) = \left[\frac{\sin(1-s(t))\Omega}{\sin(\Omega)}\right] q_{\mathrm{start}} + \left[\frac{\sin(s(t)\Omega)}{\sin(\Omega)}\right] q_{\mathrm{target}}. \tag{2}$$

Corresponding joint space trajectories are then computed by kinematic inversion in each time step [see Fig. 4(b)]. Due to the unavailability of a position reference input for RSI, a simple joint position error compensation loop with an adaptive gain has been integrated to minimize the effects of drift resulting from potentially erratic joint space commands. The compensation gain K is only active ($K = 1$) for the duration of the settling time (t_s) at the end of a P2P motion to avoid systematic error accumulation due to interference with the integral action of the proprietary industrial controller. The efficacy of this control approach is illustrated in Fig. 5. Simpler trajectory planning schemes (e.g., joint space schemes) bear the risk of incurring hardware damage and/or invalidating measurements of path-dependent effects since the corresponding Cartesian-space trajectories can cause specimen penetration beyond what is demanded throughout trajectory execution.

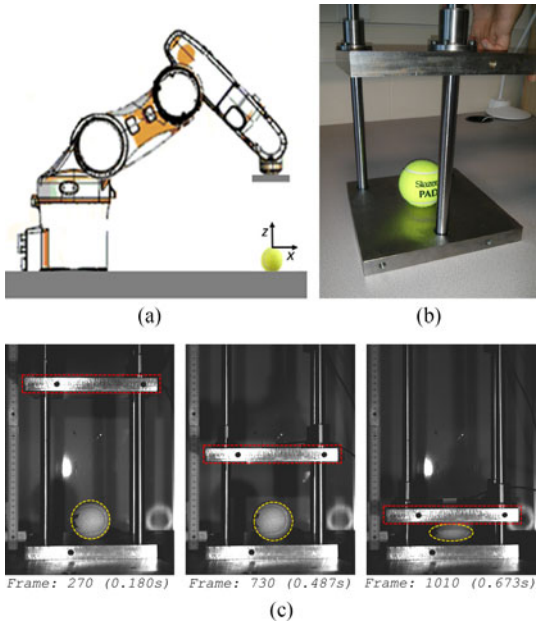

Fig. 6. (a) RPsDT setup and test reference frame. (b) Validation rig. (c) High-speed video footage of plate drop on validation rig.

III. Validation Experiments

Validation of RPsDT results is difficult, since the motivation for a hybrid test is usually based around the challenge of reproducing the full system behavior in purely experimental or purely numerical form. Without validation, however, the results of a hybrid test are unreliable. For complex tests, validation approaches must, therefore, be carefully considered on an individual basis. Here, a simple reproducible test is designed to validate the methods as a precursor to applying the technique to more complex scenarios. A specimen with significant viscous properties is included in the experimental substructure of the test to clearly outline challenges and limitations of the technique while simultaneously highlighting its strengths, and defining a subclass of contact–impact problems, to which the technique is readily applicable. To this end, a steel mass is dropped onto a spherical viscoelastic shell to validate the methodology.

A. Setup and Procedure

The basic experimental setup and test reference frame for RPsDT are illustrated in Fig. 6(a). The drop-test rig in Fig. 6(b) served the purely experimental reproduction of the contact scenario for validation purposes. Using high-speed video capture (1500 frames/s), a drop of the plate ($m = 6.50$ kg) from an initial height $z_0 = 0.205$ m ($\dot{z}_0 = 0$ m/s) was recorded. Based on manual frame-by-frame tracking of the plate's lower edge [see Fig. 6(c)], the true experimental trajectories could be extracted

from the video footage and a viscous damper model for air and rail resistance ($c = 5.18$ N/m/s) could be identified.

The RPsDT reproduction featured a point-mass model of the plate which, released from rest in a $1g$ environment and constrained to 1 DOF, drops under the combined influence of rail friction and air resistance. The viscoelastic shell (tennis ball) and plates from the validation rig (rails removed) were used as specimens in the experimental substructure and the contact force was experimentally measured by the force sensor installed between the robot end-effector and the "dropping" plate. As such, the plate's motion was governed by

$$m\ddot{z}_i = F_{c_i} - c\dot{z}_i - mg \tag{3}$$

Using a trajectory execution- and settling time of $t_{\text{exc}} = 2$ s and $t_s = 1$ s, respectively, the test procedure followed the RPsDT algorithm in Fig. 3 in its simplest from: Based on the newly acquired force measurement F_{c_i} at the start of each pseudostep, the current plate acceleration $\ddot{z}_i$ was computed from (3). The new position z_{i+1} and velocity $\dot{z}_{i+1}$ of the next time step were found by integration based on the explicit first-order Euler method using fixed step sizes of $h_s = 0.01$ ms and $h_c = 0.2$ ms throughout simulation and contact phases, respectively.

B. Results and Validation

The main drop-test results are shown in Fig. 7(a)–(c), comprising plate trajectories, force profiles for the first contact phase, as well as RPsDT-derived contact stiffness profiles of the tennis ball, respectively. All RPsDT data presented in this section are plotted against the "pseudotime," or "simulation time," rather than the true experimental time scale.

The RPsDT and experimental trajectories are shown to be in good agreement prior to the initial impact [see Fig. 7(a)], which emphasizes the validity of the friction and air resistance model in the numerical substructure throughout noncontact phases. Despite a divergence of plate trajectories thereafter and apparent differences in the contact force profiles [see Fig. 7(b)], the decisive test features in the RPsDT emulation correlate qualitatively well with those of the experimental validation test. That is, without any underlying contact model, the RPsDT method predicts:

1) successive contact scenarios with significantly damped dynamics;
2) contact force profiles that are similar to those in the experimental test with regard to shape, contact-time, as well as peak amplitude;
3) periodicity and overall frequency content comparable to experimental test data.

While such information may appear trivial for the study at hand, it can prove immediately valuable to tests of more complex systems, for which even the fundamental contact and postcontact behavior would be highly uncertain otherwise; and may provide sufficient detail to derive or enforce practically useful design changes for the tested equipment.

The increasing trajectory divergence noted above is the result of contact force discrepancies, where even minor inaccuracies can cause substantial error accumulation in the position

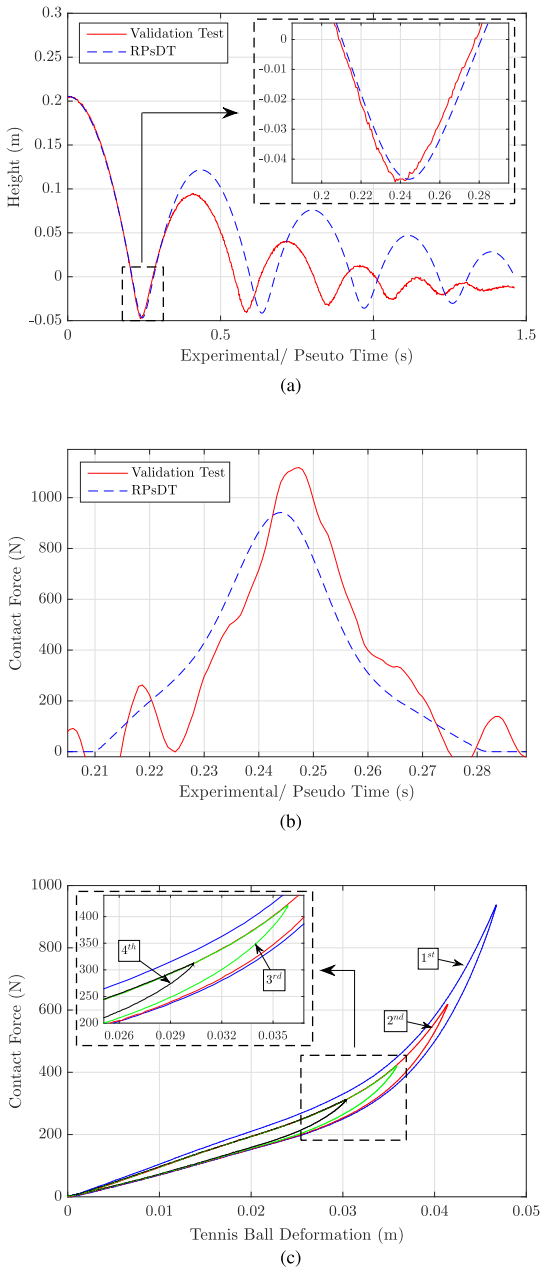

Fig. 7. (a) Experimental and RPsDT plate trajectories. (b) Contact forces on first impact. RPsDT uses direct force measurement, while experimental force is computed as a product of plate mass and acceleration (obtained by double differentiation of trajectory data) subject to application of running mean filter. (c) RPsDT contact force versus tennis ball deformation for first four contact phases.

response over time. In Fig. 7(b), the experimental contact force shows a sharper rise to a higher peak than the RPsDT force and a more asymmetric force profile, which results in a greater difference between rates of compression (faster) and restitution (slower) of the experimental data on the corresponding trajectory plot in Fig. 7(a). Both phenomena are attributed to rate-dependent damping forces captured as part of the experimental study, which contribute more significantly to the plate deceleration in compression than to a reacceleration in the restitution phase. A significant contribution to the rate-dependent

effects arises from the fluid and thermodynamic processes of the gas inside the ball: a complexity that can be avoided for a large class of systems. Due to quasi-static loading, such effects are not observable in RPsDT data, and both the RPsDT trajectory and contact force graph are consequently more symmetric. Asymmetry that is nonetheless observable in the RPsDT data is attributed to nonrate-dependent structural damping, which originates from a hysteretic, i.e., path-dependent stiffness variation that is an inherent property of the viscoelastic material. This is well pronounced in Fig. 7(c), where contact forces are plotted against deformation for all four contact phases of the recorded RPsDT data. The transition from a nominally linear elastic response to a nonlinear response is apparent at around 0.035-m deformation, with the deformation from the first impact extending far into the nonlinear region and peaking at about 90% of the ball's original diameter. In addition, it can be noted that RPsDT data show greater stiffness in the initial compression phase than throughout successive contact phases. This stiffness change does not correspond to a true RT contact phenomenon but is attributed to a time-dependent creep caused by sustained stress application over a prolonged period of time in RPsDT.

These results have promising implications with respect to hybrid simulations for AAR: The structure of the refueling drogue is predominantly elastic, and it is expected that Coulomb friction in articulated parts and hysteric damping in woven components will dominate the damping effects; these forces have correlated well in these exploratory tests. The creep effect is a minor concern, and this is mitigated as far as possible by reducing loiter times at the static equilibrium points and by screening results for such artefacts. Loiter time reductions can be achieved by replacing the constant rate orientation variation in (2) with a cubic time function subject to $s(0) = \dot{s}(0) = \dot{s}(t_{\text{exc}}) = 0$ and $s(t_{\text{exc}}) = 1$ to eliminate the infinite acceleration demands at the start and end of the motion and reduce settling time. This was implemented for the study in Section IV. Finally, good tracking accuracy can be reported for the test above, with translational and rotational errors being consistently controlled to within an apparent accuracy of 50 μm and 0.015°, respectively, subject to errors in link flexure, backlash, and forward kinematics calibration.

IV. RPsDT of Probe–Drogue Contact–Impact Scenarios in AAR

This section demonstrates the application of RPsDT to AAR maneuvers at reduced scale. While this scaling implies that none of the presented data can be regarded as representative of an actual refueling scenario, the primary focus lies on the demonstration of the capability of the underlying test method as well as the potential value for future predictions of the probe–drogue contact and coupling behavior in full-scale reproductions.

A. Physical Substructure

Resembling receiver and tanker aircraft, respectively, a KUKA KR5 sixx R650 and an ABB IRB 120 robot, are equipped with scaled probe and drogue specimens, as depicted in Fig. 1(b). Probe–drogue contact–impact scenarios are physically reproduced with both robots and coupled to numerical simulations of full-scale AAR maneuvers. To this end, interface forces measured by the FT sensor installed in-between drogue and end-effector of the ABB robot are amplified by a factor of 300 to yield a realistic effect on the simulated full-scale hose–drogue assembly upon contact, while a geometric scaling factor of 5 reduces the relative contact penetration of probe and drogue in the physical domain to avoid violation of robot workspace limits.

B. Numerical Simulation

The numerical substructure of the presented hybrid test features an AAR simulation based on previous developments detailed in [12], [20], and [21] to enable the simulation of contact-induced responses of the hose–drogue assembly in a realistic flight regime. As such, the simulation computes the relative motion of tanker, hose, drogue, and receiver aircraft as per the frame assignment in Fig. 1(a) as well as the dynamic response of the hose–drogue assembly to induced contact forces. At the start of a simulation, the hose is extended to its full pay-out length of 27 m and trailed centrally behind the tanker from a fuselage-mounted refueling pod. The hose exit point on the refueling pod is defined as the tow point and located at $p = [-21.14, 0, 0.5]$ with respect to the tanker's center of gravity that also serves as the inertial reference frame in the simulation. While the receiver aircraft follows a predefined path leading to a head-on probe–drogue collision, the flight path of the tanker is assumed undisturbed and neglects any inherent tanker dynamics. This is, over the course of the maneuver, the tanker is in straight level flight at constant altitude of 8000 m with an airspeed of 200 m/s representing an ideal docking environment. Atmospheric variations, gusts, wake, and bow wave effects are not introduced to solely highlight hose–drogue perturbations arising from contact–impact phenomena.

C. RPsDT-Based Hybrid Simulation

Off-center drogue hits are among the most critical and difficult-to-predict scenarios in AAR maneuvers. While the simulations in [20] and [21] assume that coupling attempts are instantly successful, by imposing the receiver's acceleration pattern onto the drogue immediately upon contact, the RPsDT method allows the study of the entire contact phase as well as the transition to coupling if the hit results in successful docking. This will be exemplified in the following examination of a head-on probe–drogue hit just beneath the canopy at the "12 o'clock" location. The receiver aircraft contacts the drogue at a relative speed of 1.5 m/s and decelerates to zero relative speed over 0.5 s.

The induced perturbations at the drogue's center of gravity and at the ball joint are shown in Fig. 8. Due to the specimen's large structural stiffness, the drogue does not provide for much elastic behavior but predominately reacts to the initial contact event by pivoting, i.e., tipping, about the ball joint on the Y-axis. Initially, this acts to align the relative pitch of drogue and tanker, which explains the drogue movement in the negative X-direction, i.e., away from the tanker right upon contact. As this pivoting is counteracted by both the gravitational force

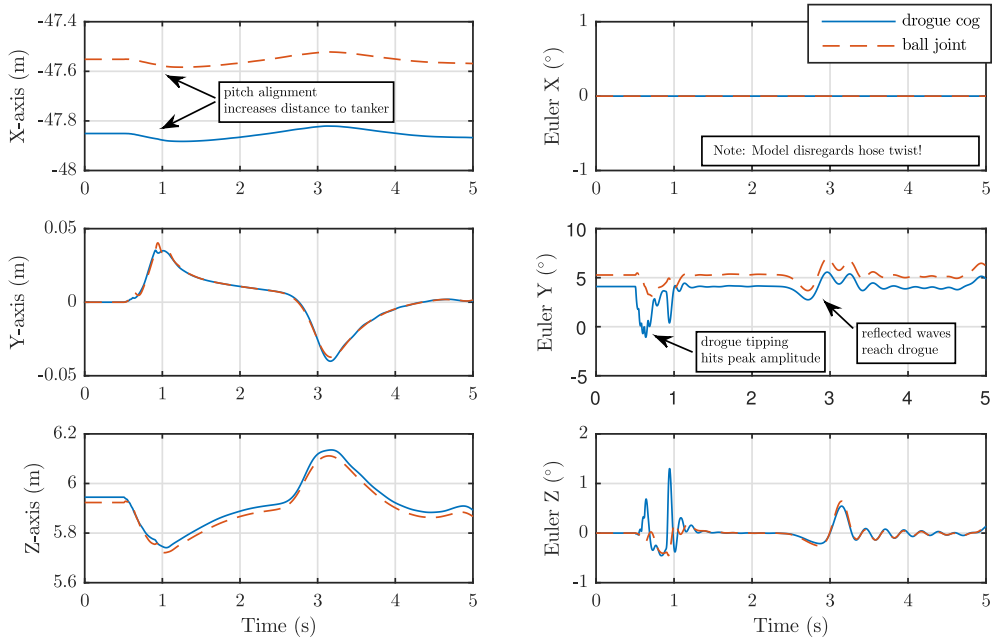

Fig. 8. Trajectory of drogue center of gravity and ball joint in a tanker reference frame.

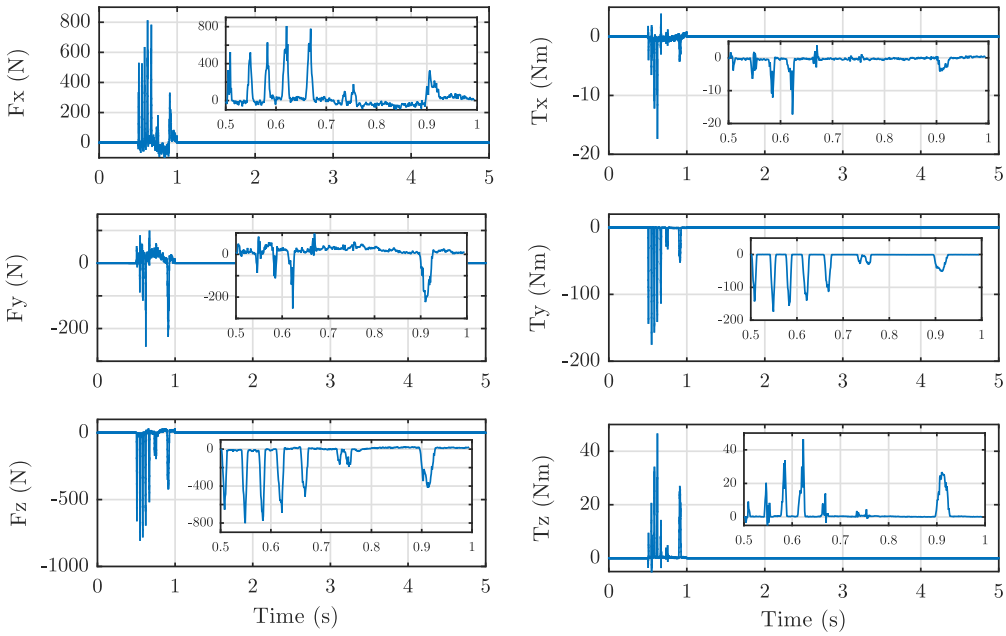

Fig. 9. Contact forces and moments in a drogue reference frame.

on the drogue and increasing aerodynamic moments, the Y-rotation reverses at a peak perturbation of about 7° to result in a rotational oscillation about the ball joint. With a minor time delay and attenuated amplitude, the ball joint follows the drogue's behavior. This is, the oscillations are also transferred onto the ball joint and further hose-upwards in the form of mechanical waves. Upon reaching the tow point, i.e., the fixed end of the hose–drogue assembly, the waves get reflected, travel down the hose, and cause a whip effect back at the drogue. Due to a viscous damping element at the ball joint, intermittent oscillations die-down quickly and make the effects of these traversing waves stand out.

The vastly discontinuous nature of the contact events becomes evident on the contact profiles in Fig. 9. Multiple losses of contact occur as the nozzle drifts increasingly toward the center of the drogue. The tipping behavior and the drogue's conical geometry contribute significantly to this. In addition, it can be noted that peak force and moments do not occur on the first impact when the relative speed is largest but on subsequent contact events instead. This is a result of the contact angle

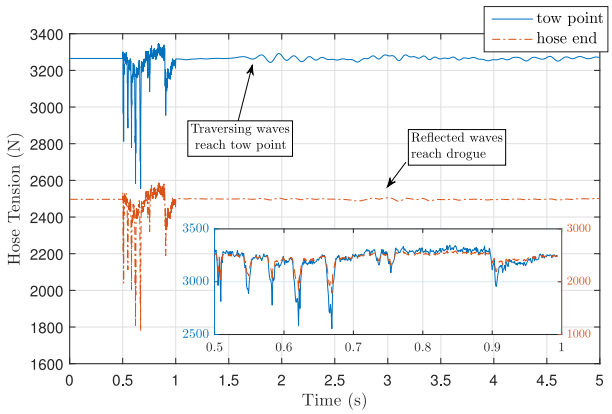

Fig. 10. Time variation of hose tension at drum exit point and hose end.

between the nozzle and the drogue that is initially steep, allowing easy slipping, but becomes increasingly more shallow as the drogue pivots. Thus, larger contact forces and moments develop at reduced relative speeds.

The induced contact forces lead to an immediate tension drop throughout the hose with following contacts resulting in further drops as the simulation progresses (see Fig. 10). At the same time, the initiation of low-frequency oscillation is recorded in the tension profiles. This is a consequence of the initial drogue rotation about the ball joint that triggers the traversing waves. While the ball-joint dampens the tension fluctuations and the aerodynamic forces and moments act to restraighten the hose–drogue assembly, the initiated waves cause persistent fluctuations as the they travel up and down the hose. In particular, prominent oscillations occur in between 2.1 and 2.6 s when the waves reach the fixed end of the hose and in between 3.2 and 3.9 s when the reflected waves cause hose whip back at the drogue.

V. Conclusion

This paper has demonstrated the feasibility of studying contact–impact problems in hybrid tests using off-the-shelf industrial robots with the robotic pseudodynamic method (RPsDT), validated both the methodology and the system architecture, and demonstrated the first hybrid simulation of docking maneuvers in AAR. The RPsDT method circumvents shortcomings in the robot response time for dynamic testing and has laid the foundation for integration of contact events into full-scale AAR simulations.

An easily reproducible validation test has shown the ability of the method to account for important nonrate-dependent effects throughout contact events including the capture of nonlinear hysteric damping characteristics. Limitations were identified to arise from the neglect of rate- and time-dependent effects, in particular those of viscous damping and creep. Shortcomings that can be addressed through improved test design have been highlighted, including the mitigation of creep effects for which careful scrutiny of results must be applied.

The RPsDT study of probe–drogue contact–impact scenarios yielded results that compared qualitatively well to phenomena known to occur in AAR maneuvers. Especially, the capture of the discontinuous contact-force profiles and drogue tipping effects that trigger much of the prominent postcontact dynamics of the hose–drogue assembly have promising implications for further investigations using the RPsDT method. Full-scale tests of more complex AAR scenarios are anticipated as future work and expected to provide further insight into the contact and postcontact behavior of the hose–drogue assembly.

References

[1] P. R. Thomas, U. Bhandari, S. Bullock, T. S. Richardson, and J. L. du Bois, "Advances in air to air refuelling," *Prog. Aerosp. Sci.*, vol. 71, pp. 14–35, Jul. 2014.

[2] J. L. duBois, P. R. Thomas, and T. S. Richardson, "Development of a relative motion facility for simulations of autonomous air to air refuelling," in *Proc. IEEE Aerosp. Conf.*, Big Sky, MT, USA, Mar. 2012, pp. 1–12.

[3] O. Ma, A. Flores-Abad, and T. Boge, "Use of industrial robots for hardware-in-the-loop simulation of satellite rendezvous and docking," *Acta Astronaut.*, vol. 81, no. 1, pp. 335–347, 2012.

[4] N. Hogan, "Impedance control: An approach to manipulation," in *Proc. IEEE Amer. Control Conf.*, 1984, pp. 304–313.

[5] R. Ortega, A. J. Van Der Schaft, I. Mareels, and B. Maschke, "Putting energy back in control," *IEEE Control Syst.*, vol. 21, no. 2, pp. 18–33, Apr. 2001.

[6] A. De Luca, "Feedforward/feedback laws for the control of flexible robots," in *Proc. IEEE Int. Conf. Robot. Autom.*, 2000, vol. 1, pp. 233–240.

[7] R. Krenn and B. Schaefer, "Limitations of hardware-in-the-loop simulations of space robotics dynamics using industrial robots," *Eur. Space Agency Publ.*, vol. 440, pp. 681–686, 1999.

[8] M. I. Wallace, D. J. Wagg, and S. A. Neild, "An adaptive polynomial based forward prediction algorithm for multi-actuator real-time dynamic substructuring," in *Proc. Roy. Soc. A, Math., Phys. Eng. Sci.*, vol. 461, no. 2064, 2005, p. 3807.

[9] T. Horiuchi, M. Inoue, T. Konno, and Y. Namita, "Real-time hybrid experimental system with actuator delay compensation and its application to a piping system with energy absorber," *Earthquake Eng. Struct. Dyn.*, vol. 28, no. 10, pp. 1121–1141, 1999.

[10] D. P. Stoten, G. Li, and J.-Y. Tu, "Model predictive control of dynamically substructured systems with application to a servohydraulically actuated mechanical plant," *IET Control Theory Appl.*, vol. 4, no. 2, pp. 253–264, Feb. 2010.

[11] A. Blomdell, I. Dressler, K. Nilsson, and A. Robertsson, "Flexible application development and high-performance motion control based on external sensing and reconfiguration of ABB industrial robot controllers," in *Proc. IEEE Int. Conf. Robot. Autom.*, 2010, pp. 62–66.

[12] J. L. du Bois, P. Thomas, S. Bullock, U. Bhandari, and T. Richardson, "Control methodologies for relative motion reproduction in a robotic hybrid test simulation of aerial refuelling," in *Proc. AIAA Guid., Navigat., Control Conf.*, Minneapolis, MN, USA, 2012, pp. 4676–4696.

[13] C. Martínez, T. Richardson, P. Thomas, J. L. duBois, and P. Campoy, "A vision-based strategy for autonomous aerial refueling tasks," *Robot. Auton. Syst.*, vol. 61, no. 8, pp. 876–895, Aug. 2013.

[14] J. L. du Bois, "A strategy for improving performance in real time hybrid testing," in *Dynamics of Civil Structures*, vol. 4. New York, NY, USA: Springer, 2014, pp. 219–225.

[15] M. Bolien, P. Iravani, and J. L. du Bois, "Robotic pseudo-dynamic testing (RPsDT) of contact-impact scenarios," in *Towards Autonomous Robotic Systems*. New York, NY, USA: Springer, 2015, pp. 50–55.

[16] S. A. Mahin and P.-S. B. Shing, "Pseudodynamic method for seismic testing," *J. Struct. Eng.*, vol. 111, no. 7, pp. 1482–1503, 1985.

[17] M. S. Williams and A. Blakeborough, "Laboratory testing of structures under dynamic loads: An introductory review," *Philosoph. Trans., Math., Phys. Eng. Sci.*, vol. 359, no. 1786, pp. 1651–1669, 2001.

[18] M. Geravand, F. Flacco, and A. De Luca, "Human-robot physical interaction and collaboration using an industrial robot with a closed control architecture," in *Proc. IEEE Int. Conf. Robot. Autom.*, 2013, pp. 4000–4007.

[19] K. Shoemake, "Animating rotation with quaternion curves," *ACM SIGGRAPH Comput. Graph.*, vol. 19, pp. 245–254, 1985.
[20] K. Ro, T. Kuk, and J. W. Kamman, "Dynamics and control of hose-drogue refueling systems during coupling," *J. Guid., Control, Dyn.*, vol. 34, no. 6, pp. 1694–1708, 2011.
[21] J. C. Vassberg, D. T. Yeh, A. J. Blair, and J. M. Evert, "Numerical simulations of KC-10 wing-mount aerial refueling hose-drogue dynamics with a reel take-up system," in *Proc. 21st Appl. Aerodyn. Conf.*, Orlando, FL, USA, 2003, vol. 26, pp. 3508–3529.

Mario Bolien received the M.Eng. degree in mechanical engineering from the University of Bath, Bath, U.K., in 2013, where he is working toward the doctoral degree.

He is an Honorary Research Associate with the University of Bristol, Bristol, U.K. He has a vast interest in the design, simulation, analysis, and control of multidomain dynamic systems. His research focuses on the development of methods and techniques for the mechanical hybrid testing of highly nonlinear and discontinuous systems, and has direct industrial relevance for the on-ground assessment of aerial refuelling hardware.

Pejman Iravani received the undergraduate degree in electrical engineering from the Universitat de Girona, Girona, Spain, in 2001, and the Ph.D. degree in distributed robot control from Open University, Milton Keynes, U.K., in 2005.

He is a Lecturer (Assistant Professor) with the Department of Mechanical Engineering, University of Bath, Bath, U.K. His research interests include robotics and autonomous systems.

Jonathan Luke du Bois received the undergraduate degree in aeronautical engineering from the University of Bristol, Bristol, U.K., in 2002, and the doctoral degree in adaptive fuselage response suppression from the Deptartment of Aerospace Engineering, University of Bristol, Bristol, U.K., in 2009.

He is a Lecturer (Assistant Professor) specializing in dynamics and control for aerospace systems with the University of Bath, Bath, U.K. He worked at the University of California, San Diego, CA, USA, before joining the University of Bath.